

# Transhydrogenation Reactions Catalyzed by Mitochondrial NADH–Ubiquinone Oxidoreductase (Complex I)<sup>†</sup>

Gregory Yakovlev and Judy Hirst\*

Medical Research Council Dunn Human Nutrition Unit, Wellcome Trust/MRC Building, Hills Road, Cambridge, CB2 0XY, U.K.

Received August 31, 2007; Revised Manuscript Received October 5, 2007

**ABSTRACT:** NADH–ubiquinone oxidoreductase (complex I) is the first enzyme of the respiratory electron transport chain in mitochondria. It conserves the energy from NADH oxidation, coupled to ubiquinone reduction, as a proton motive force across the inner membrane. Complex I catalyzes NADPH oxidation, NAD<sup>+</sup> reduction, and hydride transfers from reduced to oxidized nicotinamide nucleotides also. Here, we investigate the transhydrogenation reactions of complex I, using four different nucleotide pairs to encompass a range of reaction rates. Our experimental data are described accurately by a ping-pong mechanism with double substrate inhibition. Thus, we contend that complex I contains only one functional nucleotide binding site, in agreement with recent structural information, but in disagreement with previous mechanistic models which have suggested that two different binding sites are employed to catalyze the two half reactions. We apply the Michaelis–Menten equation to describe the productive states formed when the nucleotide and the active-site flavin mononucleotide have complementary oxidation states, and dissociation constants to describe the nonproductive states formed when they have the same oxidation state. Consequently, we derive kinetic and thermodynamic information about nucleotide binding and interconversion in complex I, relevant to understanding the mechanisms of coupled NADH oxidation and NAD<sup>+</sup> reduction, and to understanding how superoxide formation by the reduced flavin is controlled. Finally, we discuss whether NADPH oxidation and/or transhydrogenation by complex I are physiologically relevant processes.

NADH–ubiquinone oxidoreductase (complex I) is the first enzyme of the electron transport chain in mitochondria (1–4). The primary reaction catalyzed by complex I is NADH oxidation, coupled to ubiquinone reduction and to the translocation of protons across the inner mitochondrial membrane (5). Consequently, complex I is crucial for regenerating NAD<sup>+</sup> in the mitochondrial matrix, producing ubiquinol for the subsequent reactions of the electron transport chain and for contributing to the proton motive force (PMF<sup>1</sup>) which supports ATP synthesis and the transport of metabolites. When the PMF is high, relative to the potential difference between the NAD<sup>+</sup> and ubiquinone pools, complex I catalyzes in reverse: NAD<sup>+</sup> is reduced by ubiquinol, driven by the PMF (6, 7). Complex I is known to catalyze NADPH oxidation also, albeit at a much smaller rate than NADH oxidation (8). Finally, it is an important source of reactive oxygen species in mitochondria (9); superoxide is produced when O<sub>2</sub> reacts with either the reduced flavin mononucleotide (FMN) in the active site where NADH is oxidized (10) or with an ubisemiquinone radical which depends on the PMF (11).

As complex I is known to catalyze NADH and NADPH oxidation and NAD<sup>+</sup> reduction, it may catalyze transhydrogenation reactions between NAD(P)H and NAD(P)<sup>+</sup> also (eq

1). In mitochondria, transhydrogenation reactions are coupled to the PMF and catalyzed by a specific enzyme, proton-translocating transhydrogenase (12–14). Unrestrained transhydrogenation reactions in the mitochondrial matrix, catalyzed by complex I, would have obvious physiological consequences, since they would tend to equilibrate the distinct potentials of the NADP<sup>+</sup> and NAD<sup>+</sup> pools (15–19).



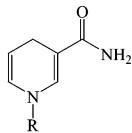
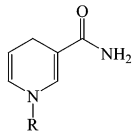
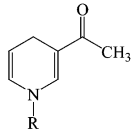
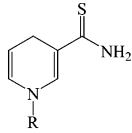
Singer and co-workers first described the transhydrogenase activity of purified complex I (20, 21). They used a variety of NAD<sup>+</sup> analogues (including APAD<sup>+</sup> and ThioNAD<sup>+</sup>) as hydride acceptors and found that, relative to NADH, NADPH is a very poor hydride donor. The rate of NADH–APAD<sup>+</sup> transhydrogenation was approximately 5% of that of NADH–ferricyanide oxidoreduction, and an estimated one-third of the total NADH–APAD<sup>+</sup> transhydrogenase activity of bovine heart mitochondria was attributed to complex I. Subsequently, Hatefi and co-workers studied submitochondrial particles and mitochondrial NADH dehydrogenase, to specify which ‘physiological’ dehydrogenase and transhydrogenase reactions may be catalyzed by complex I (8, 22, 23). Complex I was found to catalyze NAD(P)H oxidation and NAD(P)H–NAD<sup>+</sup> transhydrogenation, but it displayed little or no NAD(P)H–NADP<sup>+</sup> activity. Reactions involving NADH were significantly faster than those involving NADPH, and it was noted that, in the mitochondrion, transhydrogenation reactions involving NADP<sup>+</sup> are energy linked. Finally, Vinogradov and Zakharova have addressed

<sup>†</sup> This research was funded by The Medical Research Council.

\* Author to whom correspondence should be addressed. Tel: +44 1223 252810, fax: +44 1223 252815, e-mail: jh@mrc-dunn.cam.ac.uk.

<sup>1</sup> Abbreviations: FMN, flavin mononucleotide; HAR, hexaammineruthenium (III); FeS, iron-sulfur; LSQE, least squares error; PMF, proton motive force.

Table 1: The Nicotinamide Nucleotides Used in This Study

	Systematic name for oxidized nucleotide	Structure of nicotinamide moiety <sup>a</sup>	$E_m$ (V) (corrected to pH 7, 25 °C)	Absorbance maximum, extinction coefficient
NADH	$\beta$ -nicotinamide adenine dinucleotide		-0.32 (29)	340 nm 6.22 mM <sup>-1</sup> cm <sup>-1</sup> (30)
NADPH	$\beta$ -nicotinamide adenine dinucleotide 2'-phosphate		-0.32 (29)	340 nm 6.22 mM <sup>-1</sup> cm <sup>-1</sup> (30)
APADH	3-acetylpyridine adenine dinucleotide		-0.23 (31) -0.25 (29)	365 nm 9.1 mM <sup>-1</sup> cm <sup>-1</sup> (32)
ThioNADH	thio-nicotinamide-adenine-dinucleotide		-0.27 (31) -0.29 (33)	395 nm 11.3 mM <sup>-1</sup> cm <sup>-1</sup> (34)

<sup>a</sup> R is used to denote the ADP-ribose moiety; NADPH has an additional 2'-phosphate group on its adenosine ribose group.

the mechanism of NADH–APAD<sup>+</sup> transhydrogenation in complex I and proposed that the reaction involves two or more nucleotide binding sites (24), that it occurs by two different pathways (25), and that nucleotide binding is ordered during formation of the ternary complex (26).

Here, we study the transhydrogenation reactions catalyzed by purified complex I, using a variety of nucleotide substrates which exhibit a wide range of reaction rates. In contrast to the mechanistic models proposed previously, we contend that the reaction occurs at a single nucleotide binding site, and that it occurs with ping-pong reaction kinetics with double substrate inhibition. We define kinetic and thermodynamic constants individually for each nucleotide and for each oxidation state of the active site flavin. Thus, we further aim to determine new information about nucleotide binding to the enzyme, as a prerequisite for understanding the energy transducing NADH–ubiquinone oxidoreductase reaction and particularly for understanding how the rate of superoxide production by the reduced flavin is determined. Finally, we discuss the possibility that complex I catalyzes NADPH oxidation and/or non-energy-transducing transhydrogenation reactions in the mitochondrion.

## EXPERIMENTAL PROCEDURES

**Preparation of Complex I from Bovine Heart Mitochondria.** Complex I was prepared using the method of Sharpley and co-workers (27), with minor modifications as described by Sherwood and Hirst (28). Samples were concentrated to ~10 mg mL<sup>-1</sup> (determined using the Pierce bicinchoninic acid (BCA) assay) and frozen in liquid nitrogen for storage.

**Kinetic Measurements by UV–Visible Spectroscopy.** Assays were carried out at 32 °C in 20 mM Tris-HCl (pH 7.5),

either in cuvettes (1 mL) using a diode array spectrometer (Ocean Optics) or in 96-well plates (200  $\mu$ L) using a microtiter plate reader (Molecular Devices). The concentration of complex I was varied to give an appropriate rate for each reaction. The nicotinamide nucleotides and hexaammineruthenium III (HAR) were added from concentrated stock solutions in the assay buffer, and reactions were initiated by the addition of complex I. Initial rates were calculated using linear regression (typically over 15 s), and background rates were subtracted. The wavelengths at which the reactions were monitored were chosen according to the absorption maxima (Table 1) and concentrations of the reduced nucleotides; examples are reported in the figure legends.

**Kinetic Measurements by HPLC Analysis of the Nucleotide Composition.** Nucleotides were quantified using a modified version of the ion-pair reversed-phase HPLC method of Stocchi and co-workers (35). A 20  $\mu$ L amount of the test solution was injected onto a Hichrom 5  $\mu$ m Nucleosil C18 column (250 mm  $\times$  3.2 mm internal diameter), protected with the appropriate guard column. Buffer A contained 0.1 M potassium phosphate (pH 6) and 8 mM tetrabutylammonium hydrogen sulfate (Fisher Scientific); buffer B contained buffer A plus 30% methanol (Chromasolv, Sigma-Aldrich). The column was pre-equilibrated in 20% buffer B, and then the nucleotides were eluted at 0.5 mL min<sup>-1</sup> using the following program: 20 to 40% buffer B in 12 min, 40 to 100% buffer B in an additional 16 min, and 8 min in 100% buffer B. Elution was monitored at 254 nm, and nucleotide concentrations determined by reference to standard solutions.

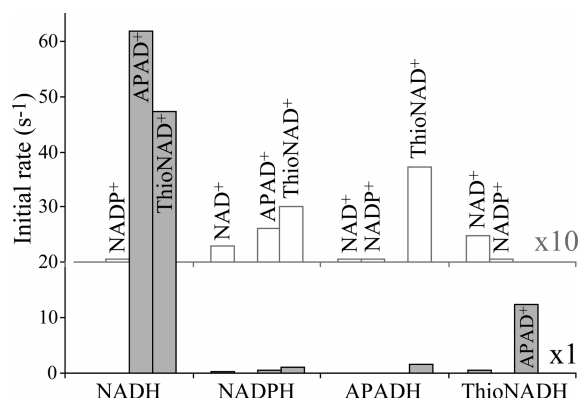


FIGURE 1: Comparison of the rates of the transhydrogenation reactions catalyzed by complex I. Initial rates ( $s^{-1}$ , moles of nucleotide converted per mole of complex I per second) were calculated by linear regression, and background rates were subtracted. Rates for the  $NADPH-NAD^{+}$  and  $NADH-NADP^{+}$  reactions were measured by HPLC analysis (see text). Solid bars refer to the ordinate scale shown; for the open bars, the values have been multiplied by ten and the bars shifted upward for clarity. Conditions: 32 °C, 20 mM Tris-HCl pH 7.5, 0.1 mM nucleotide concentration. Reactions monitored as follows:  $NAD(P)H-APAD^{+}$ ,  $\epsilon_{400-500} = 3.16 \text{ mM}^{-1} \text{ cm}^{-1}$ ;  $NAD(P)H-ThioNAD^{+}$ ,  $\epsilon_{420-500} = 8.23 \text{ mM}^{-1} \text{ cm}^{-1}$ ;  $APADH-NAD(P)^{+}$ ,  $\epsilon_{400-500} = 3.16 \text{ mM}^{-1} \text{ cm}^{-1}$ ;  $APADH-ThioNAD^{+}$ ,  $\epsilon_{440-500} = 2.38 \text{ mM}^{-1} \text{ cm}^{-1}$ ;  $ThioNADH-NAD(P)^{+}$ ,  $\epsilon_{440-500} = 2.38 \text{ mM}^{-1} \text{ cm}^{-1}$ ;  $ThioNADH-APAD^{+}$ ,  $\epsilon_{440-500} = 2.38 \text{ mM}^{-1} \text{ cm}^{-1}$ .

All analyses were performed on an Agilent 1100 system, with manual injector, column thermostat (set at 30 °C), and multiple wavelength detector, controlled by an Agilent ChemStation.

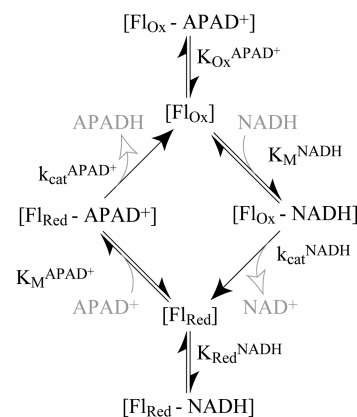
Assays for HPLC analysis were conducted under the same conditions as UV-visible assays but in the absence of  $O_2$  (see text). Using anaerobic solutions, inside a  $N_2$ -containing glovebox (Belle Technology), nucleotides were incubated in the assay buffer for 2 min (to equilibrate the temperature), the reaction was initiated with complex I, and the reaction vessel was sealed. The solution was incubated for a further 3 min, the anaerobic seal was broken, and the mixture was filtered quickly through a 0.22  $\mu\text{m}$  filter (Sartorius) and injected onto the column. It was assumed that the reaction was quenched upon injection, and the total time of incubation, including filtering and loading, was used for calculation of the reaction rate.

**Data Modeling Procedures.** Modeled curves for data fitting were calculated using either the Michaelis-Menten equation or eq 2, and the quality of the fits from different parameter combinations were assessed both by visual inspection and by calculation of least-squares error (LSQE) values (the sum of the squares of the differences between calculated and experimental data points). Fits were optimized mathematically by minimization of the LSQE values (using programs coded in C) to investigate a wide range of possible combinations of the different parameter values. When a single unique fit could not be found, combinations of parameter values which gave LSQE values below chosen limits were used to define acceptable ranges.

## RESULTS

**Complex I Catalyzes Hydride Transfer from a Reduced to an Oxidized Nucleotide.** Figure 1 presents an overview of the relative rates of the transhydrogenation reactions

Scheme 1: 'Ping-Pong' Mechanism with Double Substrate Inhibition Describing the Transhydrogenation Reactions<sup>a</sup>



<sup>a</sup>  $Fl_{Ox/Red}$ , oxidized or reduced state of the flavin;  $[ ]$ , enzyme bound species;  $k_{cat}$ , first-order rate constant for hydride transfer and product dissociation;  $K_M$ , Michaelis-Menten constant;  $K_{Ox/Red}$ , dissociation constant, referring to the oxidized or reduced state of the flavin. The model is shown for the  $NADH-APAD^{+}$  reaction but is applied to all reactions studied.

catalyzed by complex I, using four different oxidized and reduced nucleotide pairs (see Table 1) all present at a concentration of 0.1 mM. All the measurements reported are from the purified, detergent-solubilized enzyme (in the absence of a PMF). It is immediately clear that significant differences result from the nucleotide identities. When  $NADH$  is the hydride donor, rapid reactions are observed with both  $APAD^{+}$  and  $ThioNAD^{+}$ , but hydride transfer from  $NADH$  to  $NADP^{+}$  is very slow.  $APADH$  is an ineffective hydride donor, but  $APAD^{+}$  is an efficient acceptor (it has the most positive reduction potential, see Table 1).  $ThioNADH$  and  $ThioNAD^{+}$  (with an intermediate reduction potential) display reasonable reactivity in both the oxidizing and reducing directions. These observations reflect the relative thermodynamic driving forces of the reactions (see Table 1). However, reactions in which  $NADPH$  is the hydride donor are much slower than those with  $NADH$ , indicating that kinetic factors dominate in this case ( $NAD^{+}$  and  $NADP^{+}$  have the same reduction potential). Table 1 shows that  $NADH$ ,  $APADH$ , and  $ThioNADH$  differ only in their nicotinamide moieties, whereas  $NADPH$  has an additional 2'-phosphate group on the adenosine ribose moiety. Although there is no bound nucleotide present in any structural model of complex I so far, it is possible that the phosphate presents a significant barrier for access of the nicotinamide moiety to the active site, perhaps by disrupting stacking interactions between the adenine ring and aromatic residues at the entrance to the binding channel (36).

**The Mechanism of the  $NADH-APAD^{+}$  Transhydrogenation Reaction.** Figure 1 shows that the  $NADH-APAD^{+}$  reaction has the highest rate, so it was chosen as the primary subject for our mechanistic studies. Scheme 1 defines the 'ping-pong' mechanism (with double substrate inhibition) for the transhydrogenation reactions catalyzed by complex I. Crucially, it is a single site mechanism; all the nucleotides bind to the same active site, and the close match between the substrate (see Table 1) and active site flavin potentials ( $-0.38 \text{ V}$  at pH 7.5 (37)) enables the same flavin to catalyze both the oxidative and reductive half reactions. Each nucleotide may bind to both oxidation states of the flavin, and the binding constants depend on the oxidation state. Oxidized

nucleotides binding to the oxidized flavin, and reduced nucleotides binding to the reduced flavin, produce nonreactive states and are competitive inhibitors characterized by dissociation constants. Our model assumes that inhibitory nucleotide binding is fast and reversible. A reduced nucleotide binding to the oxidized flavin (and vice versa) produces a reactive state and is characterized here using the Michaelis–Menten equation and the parameters  $K_M$  and  $k_{cat}$ . Thus, our model assumes that all steps following the production of the Michaelis–Menten complex can be considered as one, and that the catalytic interconversions are irreversible (in initial rate measurements ‘back-reactions’ of the products need not be included). Finally, for simplicity, we assume that nucleotide binding and interconversion are not affected by the oxidation states of the iron-sulfur (FeS) clusters in the enzyme. Equation 2 is derived from Scheme 1 by applying the steady-state approximation to each enzyme intermediate (38), for a total complex I concentration of  $[E]_{TOT}$ .

$$\text{rate} = k_{cat}^{NADH} [F]_{Ox} - NADH = \frac{k_{cat}^{NADH} [E]_{TOT} [NADH]}{K_M^{NADH} \left( \Gamma + \Phi \frac{[NADH]}{[APAD^+]} \frac{k_{cat}^{NADH} K_M^{APAD^+}}{K_M^{NADH} k_{cat}^{APAD^+}} \right)} \quad (2)$$

where

$$\Gamma = 1 + K_{Ox}^{APAD^+} [APAD^+] + \frac{[NADH]}{K_M^{NADH}}$$

and

$$\Phi = 1 + K_{Red}^{NADH} [NADH] + \frac{[APAD^+]}{K_M^{APAD^+}}$$

Figure 2 shows how the initial rate of the NADH–APAD<sup>+</sup> reaction varies according to the concentrations of both nucleotides. The APAD<sup>+</sup> concentration dependencies are hyperbolic and dominated by the Michaelis–Menten component, whereas the NADH concentration dependencies indicate that  $k_{cat}$  is achieved at much lower NADH concentration and that, at higher concentrations, NADH becomes a competitive inhibitor, binding to the  $[F]_{Red}$  state. Figure 2 shows also a fit to the data obtained using eq 2, demonstrating clearly that the data can be explained and modeled accurately by the single-site mechanism in Scheme 1.

Equation 2 contains six independent parameters, and it was quickly found that it is not possible to define one unique set to fit the data in Figure 2. Therefore, to constrain the number of possible combinations,  $K_M$  and  $k_{cat}$  values for NADH were estimated by studying its oxidation by complex I, in conjunction with the artificial electron acceptor hexaammineruthenium (III) (HAR). Experiments were performed using high HAR concentration, so that the rate is determined as much as possible by NADH oxidation, the step common to both the oxidation and transhydrogenase reactions. Data for the NADH–HAR oxidoreductase reaction are shown in Figure 3A and were fit using the Michaelis–Menten equation; several independent experiments gave the range of values reported in Table 2. Consequently, the data shown in Figure 2 were fit using  $K_M^{NADH} = 0.094$  mM and  $k_{cat}^{NADH} = 2700$  s<sup>−1</sup>, by allowing the other four parameters to vary and

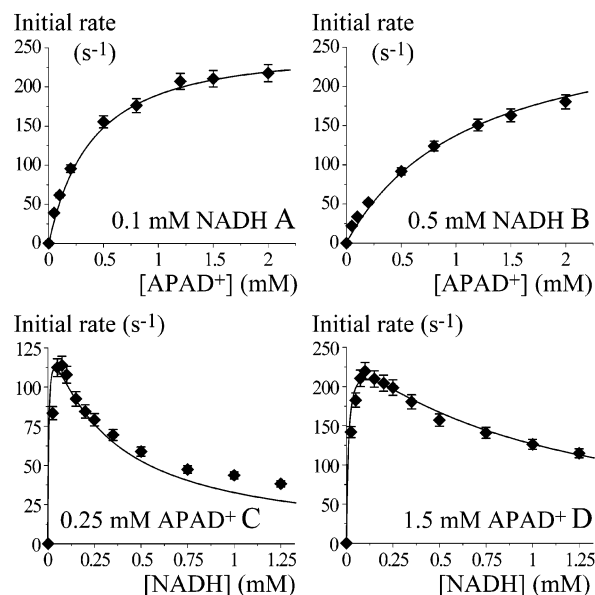


FIGURE 2: Dependence of the rate of the NADH–APAD<sup>+</sup> transhydrogenation reaction, catalyzed by complex I, on substrate nucleotide concentration. Initial rates (s<sup>−1</sup>, moles of APADH produced per mole of complex I per second) were calculated by linear regression using  $\epsilon_{400-500} = 3.16$  mM<sup>−1</sup> cm<sup>−1</sup>, and background rates were subtracted. Conditions: 32 °C, 20 mM Tris-HCl pH 7.5. ♦, experimental data points; solid lines, fit to the data using  $K_M^{NADH} = 0.094$  mM,  $k_{cat}^{NADH} = 2700$  s<sup>−1</sup>,  $K_{Red}^{NADH} = 0.16$  mM,  $K_M^{APAD^+} = 0.32$  mM,  $k_{cat}^{APAD^+} = 340$  s<sup>−1</sup>,  $K_{Ox}^{APAD^+} = 5.0$  M.

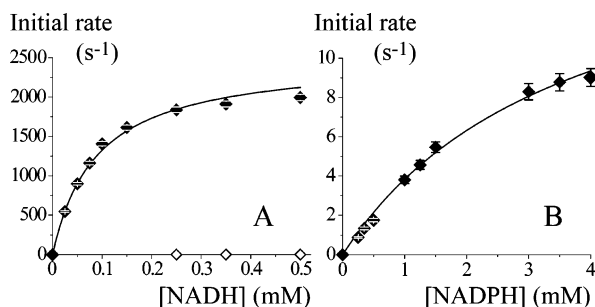


FIGURE 3: Dependence of the rate of the NADH–HAR and NADPH–HAR oxidoreductase reactions, catalyzed by complex I, on substrate nucleotide concentration at 3.5 mM HAR. Initial rates (s<sup>−1</sup>, moles of NADH or NADPH consumed per mole of complex I per second) were calculated by linear regression and background rates were subtracted. NADH oxidation:  $\epsilon_{360-400} = 4.32$  mM<sup>−1</sup> cm<sup>−1</sup>; NADPH oxidation:  $\epsilon_{370-400} = 2.75$  mM<sup>−1</sup> cm<sup>−1</sup> or  $\epsilon_{390-400} = 0.5$  mM<sup>−1</sup> cm<sup>−1</sup>. ♦, experimental data points; solid lines, fits to the Michaelis–Menten equation using  $k_{cat}^{NADH} = 2500$  s<sup>−1</sup>,  $K_M^{NADH} = 0.089$  mM,  $k_{cat}^{NADPH} = 18$  s<sup>−1</sup> and  $K_M^{NADPH} = 3.7$  mM. ◇, the data for NADPH are shown in A) for comparison.

by minimizing the LSQE. Allowing  $K_M^{NADH}$  and  $k_{cat}^{NADH}$  to vary also decreased the LSQE by approximately half (giving  $K_M^{NADH} = 0.038$  mM and  $k_{cat}^{NADH} = 500$  s<sup>−1</sup>), but visual inspection did not reveal any significant improvement in the fit quality. In addition, the quality of the fit depends most strongly on  $(k_{cat}^{NADH}/K_M^{NADH})$ ; the individual values cannot be determined with any confidence. Consequently, we chose the pragmatic approach of using the NADH–HAR oxidoreductase values for  $K_M^{NADH}$  and  $k_{cat}^{NADH}$ , to anchor our parameter search and to avoid unrealistic parameter combinations which may, in responding to imperfections in the data, give the lowest LSQE values. Finally, LSQE minimiza-



Table 2: Summary of All the Parameter Ranges Derived from Modeling the Transhydrogenation Reactions

	$K_M$ (mM)	$k_{cat}$ ( $s^{-1}$ )	$k_{cat}/K_M$ ( $s^{-1} M^{-1}$ )	$K_{Ox}$ (mM)	$K_{Red}$ (mM)
NADH	$[0.094 \pm 0.01]^a$	$[2700 \pm 200]^a$	$[2.9 \times 10^7]^a$	-	0.16–0.26
NAD <sup>+</sup>	$>0.020^b$	$>1.6^b$	$(5.0-80) \times 10^3$	$\gg 0.11^c$	-
NADPH	$[2.0-4.6]^a$	$[13-22]^a$	$[(3.0-6.5) \times 10^3]^a$	-	$\gg 0.090^c$
NADP <sup>+</sup>	$>0.14^b$	$>0.24^b$	$(0.50-1.7) \times 10^3$	$\gg 0.015^c$	-
APADH	$[0.15 \pm 0.02]^a$	$[150 \pm 20]^a$	$[1.00 \times 10^6]^a$	-	-
APAD <sup>+</sup>	0.19–0.54	290–460	$(0.78-1.7) \times 10^6$	2.8–12.5	-
ThioNADH	0.055–0.15	29–46	$(1.2-5.2) \times 10^6$	-	0.018–0.20
ThioNAD <sup>+</sup>	0.15–0.32	180–230	$(0.7-1.3) \times 10^6$	0.27–0.45	-

<sup>a</sup> Square brackets denote values from the HAR reactions, which were consistent with the modeling of the transhydrogenase reactions; the values for APADH are presented for comparison. <sup>b</sup> Only a minimum value could be established (>). <sup>c</sup> The true value is likely to be much larger than the established minimum ( $\gg$ ).

tion can always find one ‘best’ fit (whereas for the data presented in Figure 2 a variety of parameter combinations give very similar fits), and it is biased toward fitting high values at the expense of low values (whereas different criteria identify alternative best fits). Therefore, we determined parameter ranges from Figure 2, by identifying combinations which gave LSQE values below a ‘satisfactory’ threshold, set by visual inspection. The parameter ranges determined from Figure 2 were  $K_{Red}^{NADH} = 0.086-0.26$  mM,  $K_M^{APAD+} = 0.19-0.54$  mM,  $k_{cat}^{APAD+} = 290-460$  s<sup>-1</sup>, and  $K_{Ox}^{APAD+} > 0.69$  mM.

**Transhydrogenation Reactions with Different Nucleotide Combinations.** Three further transhydrogenation reactions were characterized in detail (see Figure 4). The NADH–ThioNAD<sup>+</sup> reaction is relatively fast, and, because NADH is the hydride donor in both this and the NADH–APAD<sup>+</sup> reaction, the same values of  $K_M^{NADH}$ ,  $k_{cat}^{NADH}$ , and  $K_{Red}^{NADH}$  must apply. Figures 4A,B show that (as for the NADH–APAD<sup>+</sup> reaction) the ThioNAD<sup>+</sup> dependence is hyperbolic, whereas inhibition is observed at high NADH concentrations. The data were modeled using eq 2 with  $K_M^{NADH} = 0.094$  mM,  $k_{cat}^{NADH} = 2700$  s<sup>-1</sup>, and  $K_{Red}^{NADH} = 0.086-0.26$  mM, and with the ThioNAD<sup>+</sup> parameters allowed to take any value. The satisfactory fitting approach narrowed the range for  $K_{Red}^{NADH}$  (to 0.16–0.26 mM) and defined  $K_M^{ThioNAD+} = 0.15-0.32$  mM,  $k_{cat}^{ThioNAD+} = 180-230$  s<sup>-1</sup>, and  $K_{Ox}^{ThioNAD+} = 0.27-0.45$  mM. For the ThioNADH–APAD<sup>+</sup> and NADPH–APAD<sup>+</sup> reactions (Figures 4C,D and 4E,F), the APAD<sup>+</sup> parameters must agree with those determined above, even though the reaction rates differ significantly. In both these cases inhibition is observed at high APAD<sup>+</sup> concentrations, as APAD<sup>+</sup> is able to compete with ThioNADH and NADPH for the oxidized flavin site but not with NADH (see Figure 2). The ThioNADH–HAR and NADPH–HAR (Figure 3B) reactions provided estimates of  $K_M^{ThioNADH} = 0.045-0.12$  mM,  $k_{cat}^{ThioNADH} = 63-86$  s<sup>-1</sup>,  $K_M^{NADPH} = 2.0-4.6$  mM, and  $k_{cat}^{NADPH} = 13-22$  s<sup>-1</sup>. These ranges were not modified, except that it was necessary to decrease  $k_{cat}^{ThioNADH}$  by approximately 50% (to 29–46 s<sup>-1</sup>) and to increase  $K_M^{ThioNADH}$  slightly (to 0.055–0.15 mM) to achieve a satisfactory fit to Figures 4C,D.  $K_{Red}^{ThioNADH}$  and  $K_{Red}^{NADPH}$  were allowed to take any value and were found to be 0.018–0.2 mM and  $>0.09$  mM, respectively. The ranges for  $K_M^{APAD+}$  and  $k_{cat}^{APAD+}$  were unchanged, but that for  $K_{Ox}^{APAD+}$  was narrowed to 2.8–12.5 mM.

**The NADH–NADP<sup>+</sup> and NADPH–NAD<sup>+</sup> Transhydrogenation Reactions Studied by HPLC Analysis.** Transhydro-

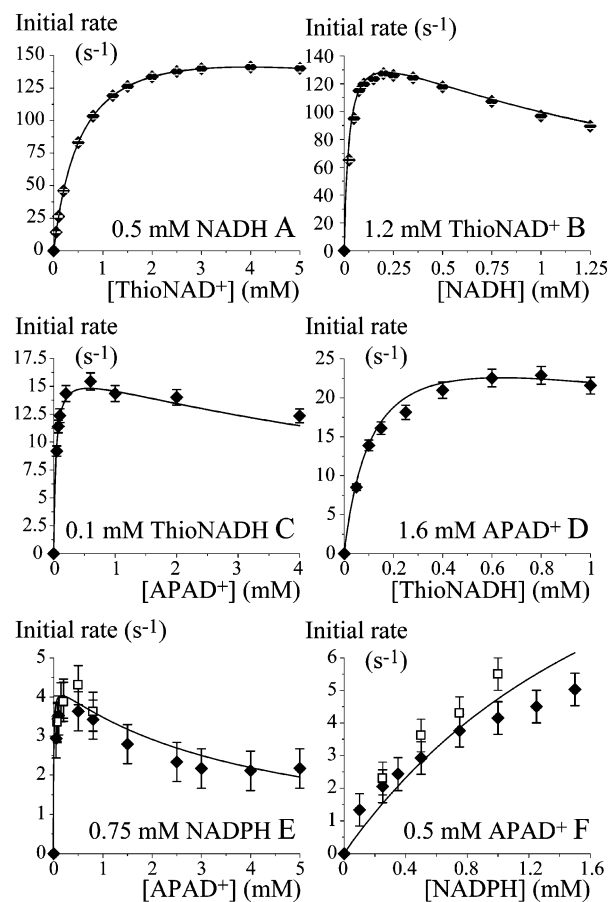


FIGURE 4: Dependence of the rate of various transhydrogenation reactions, catalyzed by complex I, on substrate nucleotide concentration. Initial rates ( $s^{-1}$ , moles of ThioNADH produced (A and B,  $\epsilon_{420-500} = 8.23$  mM<sup>-1</sup> cm<sup>-1</sup>), ThioNADH consumed (C and D,  $\epsilon_{440-500} = 2.38$  mM<sup>-1</sup> cm<sup>-1</sup>), or APADH produced (E and F,  $\epsilon_{400-500} = 3.16$  mM<sup>-1</sup> cm<sup>-1</sup>), per mole of complex I per second) were calculated by linear regression, and background rates were subtracted. Conditions: 32 °C, 20 mM Tris-HCl pH 7.5.  $\blacklozenge$ , experimental data points; solid lines, fit to the data using:  $K_M^{NADH} = 0.094$  mM,  $k_{cat}^{NADH} = 2700$  s<sup>-1</sup>,  $K_{Red}^{NADH} = 0.25$  mM,  $K_M^{ThioNAD+} = 0.22$  mM,  $k_{cat}^{ThioNAD+} = 200$  s<sup>-1</sup>,  $K_{Ox}^{ThioNAD+} = 0.33$  mM (A and B);  $K_M^{ThioNADH} = 0.095$  mM,  $k_{cat}^{ThioNADH} = 34$  s<sup>-1</sup>,  $K_{Red}^{ThioNADH} = 0.055$  mM,  $K_M^{APAD+} = 0.31$  mM,  $k_{cat}^{APAD+} = 400$  s<sup>-1</sup>,  $K_{Ox}^{APAD+} = 4.2$  mM (C and D);  $K_M^{NADPH} = 2.3$  mM,  $k_{cat}^{NADPH} = 18$  s<sup>-1</sup>,  $K_{Red}^{NADPH} = 1.0$  mM,  $K_M^{APAD+} = 0.33$  mM,  $k_{cat}^{APAD+} = 350$  s<sup>-1</sup>,  $K_{Ox}^{APAD+} = 3.0$  mM (E and F). In E and F, the additional data points ( $\square$ ) are from equivalent measurements by HPLC analysis (see text).

genation reactions between NAD(H) and NADP(H) are spectroscopically invisible because the UV–visible spectra of NADH and NADPH are the same (30). However, all the

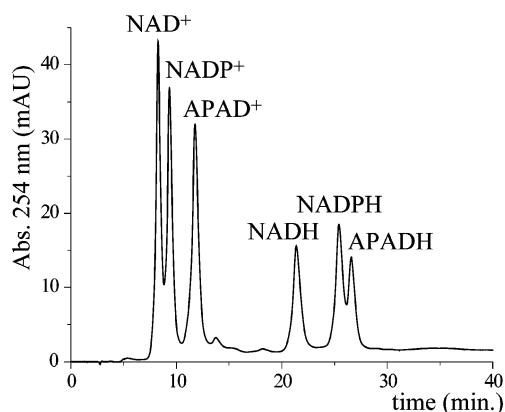


FIGURE 5: HPLC analysis of a nucleotide mixture. The nucleotides were all present at 50  $\mu$ M. The small extra peak observed at 14 min was an undefined impurity present in APADH. Conditions: 5  $\mu$ m Nucleosil C18 column (250 mm  $\times$  3.2 mm), injection volume 20  $\mu$ L, elution at 0.5 mL min<sup>-1</sup> in 0.1 M potassium phosphate (pH 6) containing 8 mM tetrabutylammonium hydrogen sulfate with a gradient of 6–30% methanol (see Experimental Procedures).

reactions of NADPH and NADP<sup>+</sup> are slow (see Figure 1), so that HPLC analysis, at a fixed time point, can be used to determine their rates.

Figure 5 shows a typical HPLC trace, quantifying the different nucleotides in a mixture. Analysis of standard solutions (0 to 1 mM) confirmed that the elution peak areas varied linearly with concentration, and that concentrations down to 2  $\mu$ M could be determined. First, our methodology was established using the NADPH–APAD<sup>+</sup> reaction, and Figure 4F includes data points from both HPLC and UV–visible assays, confirming their close agreement. In all cases, preliminary experiments were used to confirm that the 3 min time point used was within the linear phase of the reaction, enabling the initial rate to be determined. All the reactions were carried out under anaerobic conditions, because their turnover rates are so slow that O<sub>2</sub> competes efficiently for the reduced flavin (10), leading to nonstoichiometric changes in nucleotide concentration. In preliminary experiments, all four nucleotide concentrations were quantified, but only the two products were used in routine analysis, since the high reactant concentrations gave very small percentage changes and thus higher errors. Finally, the NADH–NADP<sup>+</sup> and NADPH–NAD<sup>+</sup> reactions are extremely slow, so that relatively large amounts of enzyme are required, limiting the number of assays that could be carried out.

Figures 6A,B show data for the NADPH–NAD<sup>+</sup> transhydrogenase reaction. Consistent with a high value for  $K_M^{\text{NADPH}}$ , the dependence on NADPH concentration is hyperbolic, whereas mild inhibition is observed at the highest NAD<sup>+</sup> concentration. The data were modeled using  $K_M^{\text{NADPH}} = 2.0\text{--}4.6$  mM,  $k_{\text{cat}}^{\text{NADPH}} = 13\text{--}22$  s<sup>-1</sup>, and  $K_{\text{Red}}^{\text{NADPH}} > 0.09$  mM (see above), and the NAD<sup>+</sup> parameters were allowed to take any value. Because of the limited datasets available, the NADPH parameters were not refined further, and screening for satisfactory values of  $K_M^{\text{NAD}^+}$ ,  $k_{\text{cat}}^{\text{NAD}^+}$ , and  $K_{\text{ox}}^{\text{NAD}^+}$  resulted in wide ranges, for which only minimum values could be established.  $K_{\text{ox}}^{\text{NAD}^+} > 0.11$  mM could adopt values as high as 1 M without compromising the fit. Similarly,  $K_M^{\text{NAD}^+} > 0.02$  mM and  $k_{\text{cat}}^{\text{NAD}^+} > 1.6$  s<sup>-1</sup> could be far higher than their minimum values (for example, 100 mM and 600 s<sup>-1</sup> respectively). However, a relationship was

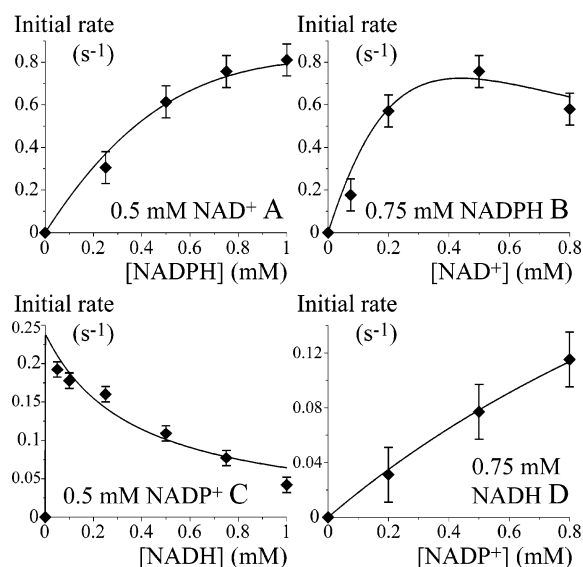


FIGURE 6: Dependence of the rate of the NADPH–NAD<sup>+</sup> and NADH–NADP<sup>+</sup> transhydrogenation reactions, catalyzed by complex I, on substrate nucleotide concentration. Initial rates (s<sup>-1</sup>, moles of each product produced per mole of complex I per second) were calculated from HPLC analysis of the nucleotide concentrations as described in the text. Conditions: 32 °C, 20 mM Tris-HCl pH 7.5. ♦, experimental data points; solid lines, fit to the data using  $K_M^{\text{NADPH}} = 2.4$  mM,  $k_{\text{cat}}^{\text{NADPH}} = 18$  s<sup>-1</sup>,  $K_{\text{Red}}^{\text{NADPH}} = 0.54$  mM,  $K_M^{\text{NAD}^+} = 0.95$  mM,  $k_{\text{cat}}^{\text{NAD}^+} = 10$  s<sup>-1</sup>,  $K_{\text{ox}}^{\text{NAD}^+} = 0.16$  mM (A and B);  $K_M^{\text{NADH}} = 0.094$  mM,  $k_{\text{cat}}^{\text{NADH}} = 2700$  s<sup>-1</sup>,  $K_{\text{Red}}^{\text{NADH}} = 0.18$  mM,  $K_M^{\text{NADP}^+} = 0.48$  mM,  $k_{\text{cat}}^{\text{NADP}^+} = 0.47$  s<sup>-1</sup>,  $K_{\text{ox}}^{\text{NADP}^+} = 1.0$  mM (C and D).

observed between  $K_M^{\text{NAD}^+}$  and  $k_{\text{cat}}^{\text{NAD}^+}$ , and, using the satisfactory fitting approach, a range for ( $k_{\text{cat}}^{\text{NAD}^+}/K_M^{\text{NAD}^+}$ ) was obtained ( $k_{\text{cat}}^{\text{NAD}^+}/K_M^{\text{NAD}^+} = (5\text{--}80) \times 10^3$  s<sup>-1</sup> M<sup>-1</sup>). For the NADH–NADP<sup>+</sup> reaction (Figures 6C,D), the expected inhibition from NADH is observed, while the dependence on NADP<sup>+</sup> concentration is hyperbolic. The data were modeled using  $K_M^{\text{NADH}} = 0.094$  mM,  $k_{\text{cat}}^{\text{NADH}} = 2700$  s<sup>-1</sup>, and  $K_{\text{Red}}^{\text{NADH}} = 0.16\text{--}0.26$  mM (determined above), with the NADP<sup>+</sup> parameters allowed to take any value. Again, many different parameter combinations gave satisfactory fits, consistent with the linear dependence on NADP<sup>+</sup> concentration and the lack of NADP<sup>+</sup> inhibition. The true value for  $K_{\text{ox}}^{\text{NADP}^+}$  is anticipated to be significantly above its established minimum, 0.015 mM. Only minimum values could be established for  $K_M^{\text{NADP}^+}$  and  $k_{\text{cat}}^{\text{NADP}^+}$  ( $K_M^{\text{NADP}^+} > 0.14$  mM,  $k_{\text{cat}}^{\text{NADP}^+} > 0.24$  s<sup>-1</sup>), and a relationship between  $K_M^{\text{NADP}^+}$  and  $k_{\text{cat}}^{\text{NADP}^+}$  was again observed, as both parameters could go to much higher values (for example, 100 mM and 50 s<sup>-1</sup>) without affecting the LSQE value. The range established for ( $k_{\text{cat}}^{\text{NADP}^+}/K_M^{\text{NADP}^+}$ ), of  $(0.5\text{--}1.7) \times 10^3$  s<sup>-1</sup> M<sup>-1</sup>, was lower in magnitude than the corresponding range for NAD<sup>+</sup>.

## DISCUSSION

*The Mechanism of Transhydrogenation by Complex I.* All the transhydrogenation reactions catalyzed by complex I were modeled successfully using the single-site ping-pong mechanism with double substrate inhibition, and reactions with common substrates were modeled with common parameter sets (final parameter ranges are summarized in Table 2).

Clearly, comparing data from different nucleotide combinations provides more robust parameter sets, and a more stringent test of our reaction mechanism, than only a single combination. We conclude that the single-site mechanism of Scheme 1 is a simple and sufficient model for the transhydrogenation reaction, and it is not necessary to propose the existence of multiple nucleotide binding sites in complex I. Although it combines hydride transfer and nucleotide dissociation into a single irreversible step (so is not completely comprehensive), it has allowed the determination of parameter ranges for future refinement and further investigations. Finally, our mechanism is clearly distinct from that of transhydrogenase itself (13, 14). Transhydrogenase does not require an additional cofactor, such as the complex I flavin, to shuttle the hydride moiety. Instead, direct hydride transfer between the two nicotinamide rings occurs in a ternary complex, and conformational changes link hydride transfer to the PMF to prevent the enzyme 'free wheeling'.

Previous studies by Vinogradov and Zakharova concluded that, in complex I, NADH-APAD<sup>+</sup> transhydrogenation requires two distinct nucleotide binding sites (24–26). Clearly, their dual-site model is incompatible with the single-site model presented here. It is possible that the disagreement arises because the previous studies relied on double-reciprocal plot analysis. Here, we chose the more intuitive direct analysis, because the double-reciprocal form of eq 2 is nonlinear (unless limiting approximations are taken), confounding the interpretation of double-reciprocal plots and providing no analytical advantage. Indeed, it was reported that double-reciprocal plots in regions 'where the substrate inhibition could be neglected' were either curvilinear, or they intersected in different quadrants depending on substrate concentration (24, 25). Although such observations were taken to suggest complex kinetics and more than one binding site, they are consistent with the double-reciprocal form of eq 2. Furthermore, using the mechanism from Scheme 1 and the parameters from Table 2, we were able to generate modeled data showing excellent qualitative agreement with the previously reported experimental data (24, 25).

Knowledge of the number of substrate binding sites is a prerequisite for understanding the mechanism of an enzyme. A single nucleotide binding site was identified in the Nqo1 subunit in the structure of the hydrophilic domain of complex I from *T. thermophilus* (36), consistent with earlier labeling studies which showed that the bovine 51 kDa subunit contains an NADH binding site (39). Although NADPH binds to the 39 kDa subunit in bovine and *Yarrowia lipolytica* complex I (40, 41), the 39 kDa subunit is supernumerary (42) so the bound NADPH is probably spatially and functionally separate from the redox machinery. Indeed, no catalytic function has been identified for it, and in a form of *Y. lipolytica* complex I that lacks the 51 and 24 kDa subunits (but retains the 39 kDa subunit) the iron-sulfur (FeS) clusters were not reduced by NADH or NADPH (43). We note that further evidence to support more than one catalytic nucleotide binding site in complex I has been presented. It includes different FeS cluster reduction patterns upon the treatment of complex I with NADPH or NADH (44). However, similar data has been explained by the slow NADPH dehydrogenation rate and enzyme autooxidation (45), and when the positions of the clusters were defined (36), it became clear that electrons should pass easily between them, precluding

the reduction of different subsets by different nucleotides. It also includes observations of nucleotides, acting as either inhibitors or substrates, displaying different affinities in 'forward' or 'reverse' electron-transfer reactions (46, 47). However, we propose a simpler and more robust explanation, that the oxidation state of the active site flavin differs according to the 'direction' of the reaction, and that this defines the nucleotide affinities.

**Nucleotide Binding and Kinetic Constants.** Scheme 1 and Table 2 show that very different reaction rates are produced by competition for the nucleotide binding site, tempered by its specificity, the 'productive'  $K_M$  and  $k_{cat}$  versus the 'inhibitory'  $K_{Ox/Red}$ .

(i) For the reduced nucleotides,  $k_{cat}^{NADH} > (k_{cat}^{APADH}, k_{cat}^{ThioNADH}) > k_{cat}^{NADPH}$  (see Table 2), indicating that, especially for NADPH, either hydride transfer or product dissociation is slow. Within the active site, steric interactions may hinder the stacking of the nicotinamide and isoalloxazine rings required for hydride transfer. In transhydrogenase, subtle effects on the conformational changes which produce the ground state for hydride transfer have recently been revealed in studies of thionicotinamide nucleotide analogues (48). For NADPH, the additional phosphate may disrupt interactions between the adenine rings and aromatic residues at the entrance to the NADH-binding cavity (36), preventing the nicotinamide headgroup attaining the correct position.

(ii) Because  $K_M = (k_{off} + k_{cat})/k_{on}$  (where  $k_{on}$  and  $k_{off}$  describe the reactant nucleotide binding and dissociating), the magnitude of  $k_{cat}$  affects  $K_M$ . However, NADPH has the smallest  $k_{cat}$  and the largest  $K_M$  of any reduced nucleotide, indicating that the rate of nucleotide binding is a second key determinant of the turnover rate. Furthermore, the specificity constant ( $k_{cat}/K_M$ ) for NADH is 4 orders of magnitude higher than for NADPH, and one order higher than for APADH and ThioNADH (Table 2): an encounter between the oxidized enzyme and NADH is much more likely to produce a reactive complex than an encounter with NADPH. In fact,  $(k_{cat}^{NADH}/K_M^{NADH})$  is close to the diffusion controlled limit and comparable to the values of acetyl cholinesterase ( $1.6 \times 10^8 \text{ M}^{-1} \text{ s}^{-1}$ ), carbonic anhydrase ( $1.5\text{--}8.3 \times 10^7 \text{ M}^{-1} \text{ s}^{-1}$ ), and catalase ( $4 \times 10^7 \text{ M}^{-1} \text{ s}^{-1}$ ) (49).

(iii) The  $K_M$  values in Table 2 do not provide direct information about the substrate dissociation constants, because  $K_M \rightarrow K_D$  only if  $k_{off} \gg k_{cat}$ , and the  $k_{cat}$  values are too high. However,  $K_M$  defines the upper limit of  $K_D$ . Thus, NADH binds more tightly when the flavin is oxidized ( $K_D < 0.094 \text{ mM}$ ) than when it is reduced ( $K_{Red} = 0.16$  to  $0.26 \text{ mM}$ ), whereas APAD<sup>+</sup> binds more tightly when it is reduced ( $K_D < 0.19$  to  $0.54 \text{ mM}$  versus  $K_{Ox} = 2.8$  to  $12.5 \text{ mM}$ ). The oxidation-state-dependent binding of APAD<sup>+</sup> may reflect the behavior of NAD<sup>+</sup> (for which only very limited information is available), but we note that the four binding constants for ThioNAD<sup>+</sup> and ThioNADH do not vary significantly.

There is little published data for comparison with the data in Table 2. By considering complex I catalyzed NADH-WB oxidoreduction (WB, Wurster's Blue, *N,N,N',N'*-tetramethyl-*p*-phenylenediamine), Avraam and Kotlyar used the limit of  $K_M \rightarrow K_D$  as  $V_{max} \rightarrow 0$  (determined by the WB concentration) and reported that  $K_D^{NADH} = 0.17 \text{ } \mu\text{M}$  (50). Inhibition by NAD<sup>+</sup> gave  $K_I^{NAD+} = 1.6 \text{ mM}$  (we expect  $K_I^{NAD+} \approx K_{Ox}^{NAD+}$ ). They further determined  $K_M^{NAD+} = 25$



$\mu\text{M}$  and  $K_I^{\text{NADH}} = 80 \mu\text{M}$  ( $\approx K_{\text{Red}}^{\text{NADH}}$ ) during ATP-dependent reverse electron transport in submitochondrial particles, and proposed that  $k_{\text{cat}}$  is slow so that  $K_M^{\text{NAD}^+} \approx K_D^{\text{NAD}^+}$ . Similarly, but using HAR as the electron acceptor, Sled and Vinogradov reported  $K_D^{\text{NADH}} = 40 \mu\text{M}$  and  $K_I^{\text{NAD}^+} = 2.0 \text{ mM}$  (51), and by studying ATP-dependent reverse electron transport,  $K_D^{\text{NAD}^+} = 0.9 \mu\text{M}$  and  $K_I^{\text{NADH}} = 40 \mu\text{M}$  (47). Although it is obvious that the two  $K_D^{\text{NADH}}$  and  $K_D^{\text{NAD}^+}$  values differ significantly, the data in Table 2 are consistent with both sets of values, and good agreement is observed between values for  $K_{\text{Red}}^{\text{NADH}}$  (160–260  $\mu\text{M}$ , Table 2) and  $K_I^{\text{NADH}}$  (40 and 80  $\mu\text{M}$ , see above). Finally, we note that using reverse electron transport, driven by the PMF, to study the kinetics of  $\text{NAD}^+$  reduction, is a significant challenge, both experimentally and theoretically. Though not a focus of the current work,  $\text{NAD}^+$  reduction driven by transhydrogenation may provide an alternative, simpler, approach.

**Does Complex I Catalyze Transhydrogenation Reactions in Mitochondria?** In mitochondria, the  $\text{NAD}^+$  and  $\text{NADP}^+$  potentials are held at different values; the  $\text{NAD}^+$  pool is predominantly oxidized, whereas the  $\text{NADP}^+$  pool is predominantly reduced (12, 15–19). Because transhydrogenation by complex I is not energy transducing and so not controlled by the PMF, complex I could, in principle, catalyze ‘downhill’ hydride transfer from  $\text{NADPH}$  to  $\text{NAD}^+$ , to collapse the  $\text{NADP}^+$  potential. Consequently, re-establishing the  $\text{NADP}^+$  potential, most obviously by the transhydrogenase enzyme using the PMF to drive the reverse reaction, would complete an energetically wasteful, futile cycle (12). Mitochondrial  $\text{NADPH}$  is important in, for example, maintaining the glutathione pool potential to minimize oxidative damage, fatty acid and steroid synthesis, and as a substrate for enzymes such as glutamate dehydrogenase (12, 52, 53).

On the basis of estimated potentials and concentrations for  $\text{NAD(H)}$  and  $\text{NADP(H)}$  in the mitochondrial matrix (12, 15–19), we consider transhydrogenation by complex I in the presence of 0.3 mM  $\text{NADH}$ , 3 mM  $\text{NAD}^+$ , 3 mM  $\text{NADPH}$ , and 0.03 mM  $\text{NADP}^+$ . The parameters in Table 2 indicate that  $\text{NADH}$  heavily out-competes  $\text{NADPH}$  for the complex I active site, with less than 0.2% of the dehydrogenation reactions attributed to  $\text{NADPH}$ . Once the flavin is reduced,  $\text{NAD}^+$  (and  $\text{NADP}^+$ ) compete with ubiquinone for the electron pair, and with  $\text{NADH}$  (and  $\text{NADPH}$ ) for the active site. Transhydrogenation will only occur if  $\text{NAD}^+$  binds to complex I and is reduced, since  $\text{NADP}^+$  reduction would re-form  $\text{NADPH}$ , and the reduction of ubiquinone (or the binding of  $\text{NADH}$  to the reduced flavin, blocking the active site until ubiquinone is reduced) would result in one turnover of  $\text{NADPH}$ –ubiquinone oxidoreduction. Thus, our results suggest that the strong specificity of complex I for  $\text{NADH}$  (rather than  $\text{NADPH}$ ) is the predominant way in which significant transhydrogenation is prevented, aided by the minimization of  $\text{NAD}^+$  (or  $\text{NADP}^+$ ) reduction, by  $\text{NADH}$  binding to the reduced flavin and by ubiquinone reduction. It is likely that a small amount of  $\text{NADPH}$ –ubiquinone oxidoreduction occurs physiologically and is tolerated or compensated for.

## REFERENCES

- Walker, J. E. (1992) The  $\text{NADH}$ –ubiquinone oxidoreductase (complex I) of respiratory chains, *Q. Rev. Biophys.* 25, 253–324.
- Yagi, T., and Matsuno-Yagi, A. (2003) The proton-translocating  $\text{NADH}$ –ubiquinone oxidoreductase in the respiratory chain: the secret unlocked, *Biochemistry* 42, 2266–2274.
- Hirst, J. (2005) Energy transduction by respiratory complex I – an evaluation of current knowledge, *Biochem. Soc. Trans.* 33, 525–529.
- Sazanov, L. A. (2007) Respiratory complex I: mechanistic and structural insights provided by the crystal structure of the hydrophilic domain, *Biochemistry* 46, 2275–2288.
- Wikström, M. (1984) Two protons are pumped from the mitochondrial matrix per electron transferred between  $\text{NADH}$  and ubiquinone, *FEBS Lett.* 169, 300–304.
- Chance, B., and Hollunger, G. (1961) The interaction of energy and electron transfer reactions in mitochondria, *J. Biol. Chem.* 236, 1534–1543.
- Chance, B., Lees, H., and Postgate, J. R. (1972) The meaning of “reversed electron flow” and “high energy electron” in biochemistry, *Nature* 238, 330–331.
- Hatefi, Y., and Galante, Y. M. (1977) Dehydrogenase and transhydrogenase properties of the soluble  $\text{NADH}$  dehydrogenase of bovine heart mitochondria, *Proc. Natl. Acad. Sci. U.S.A.* 74, 846–850.
- Brand, M. D., Affourtit, C., Esteves, T. C., Green, K., Lambert, A. J., Miwa, S., Pakay, J. L., and Parker, N. (2004) Mitochondrial superoxide: production, biological effects, and activation of uncoupling proteins, *Free Rad. Biol. Med.* 37, 755–767.
- Kussmaul, L., and Hirst, J. (2006) The mechanism of superoxide production by  $\text{NADH}$ :ubiquinone oxidoreductase from bovine heart mitochondria, *Proc. Natl. Acad. Sci. U.S.A.* 103, 7607–7612.
- Lambert, A. J., and Brand, M. D. (2004) Superoxide production by  $\text{NADH}$ :ubiquinone oxidoreductase (complex I) depends on the pH gradient across the mitochondrial inner membrane, *Biochem. J.* 382, 511–517.
- Hoek, J. B., and Rydström, J. (1988) Physiological roles of nicotinamide nucleotide transhydrogenase, *Biochem. J.* 254, 1–10.
- Jackson, J. B., White, S. A., Quirk, P. G., and Venning, J. D. (2002) The alternating site, binding change mechanism for proton translocation by transhydrogenase, *Biochemistry* 41, 4173–4185.
- Jackson, J. B. (2003) Proton translocation by transhydrogenase, *FEBS Lett.* 545, 18–24.
- Bücher, T., and Sies, H. (1976) Mitochondrial and cytosolic redox states in perfused rat liver: methods and problems in metabolic compartmentation, in *Use of isolated liver cells and kidney tubules in metabolic studies* (Tager, J. M., Söling, H. D., and Williamson, J. R., Eds.) pp 41–64, North-Holland Publishing Company, Amsterdam.
- Tischler, M. E., Friedrichs, D., Coll, K., and Williamson, J. R. (1977) Pyridine nucleotide distributions and enzyme mass action ratios in hepatocytes from fed and starved rats, *Arch. Biochem. Biophys.* 184, 222–236.
- Williamson, J. R., and Corkey, B. E. (1979) Assay of citric acid cycle intermediates and related compounds – update with tissue metabolite levels and intracellular distribution, *Methods Enzymol.* 55, 200–222.
- Sies, H. (1982) Nicotinamide nucleotide compartmentation, in *Metabolic compartmentation* (Sies, H., Ed.) pp 205–231, Academic Press, London.
- Nicholls, D. G., and Ferguson, S. J. (2002) *Bioenergetics* 3, Academic Press, London.
- Minakami, S., Ringler, R. L., and Singer, T. P. (1962) Studies on the respiratory chain-linked dihydridophosphopyridine nucleotide dehydrogenase, *J. Biol. Chem.* 237, 569–576.
- Minakami, S., Cremona, T., Ringler, R. L., and Singer, T. P. (1963) Studies on the respiratory chain-linked reduced nicotinamide adenine dinucleotide dehydrogenase, *J. Biol. Chem.* 238, 1529–1537.
- Hatefi, Y., and Hanstein, W. G. (1973) Interactions of reduced and oxidized triphosphopyridine nucleotides with the electron-transport system of bovine heart mitochondria, *Biochemistry* 12, 3515–3522.
- Djavadi-Ohanian, L., and Hatefi, Y. (1975) Oxidation of  $\text{NADPH}$  by submitochondrial particles from beef heart in complete absence of transhydrogenase activity from  $\text{NADPH}$  to  $\text{NAD}$ , *J. Biol. Chem.* 250, 9397–9403.
- Zakharova, N. V., Zharova, T. V., and Vinogradov, A. D. (1999) Kinetics of transhydrogenase reaction catalyzed by the mitochon-



- drial NADH-ubiquinone oxidoreductase (complex I) imply more than one catalytic nucleotide-binding sites, *FEBS Lett.* 444, 211–216.
25. Zakharova, N. V. (2002) Kinetics of the transhydrogenase reaction catalyzed by mitochondrial NADH:ubiquinone oxidoreductase (complex I), *Biochemistry (Mosc.)* 67, 651–661.
26. Zakharova, N. V., and Zharova, T. V. (2002) Kinetic mechanism of mitochondrial NADH:ubiquinone oxidoreductase interaction with nucleotide substrates of the transhydrogenase reaction, *Biochemistry (Mosc.)* 67, 1395–1404.
27. Sharpley, M. S., Shannon, R. J., Draghi, F., and Hirst, J. (2006) Interactions between phospholipids and NADH:ubiquinone oxidoreductase (complex I) from bovine mitochondria, *Biochemistry* 45, 241–248.
28. Sherwood, S., and Hirst, J. (2006) Investigation of the mechanism of proton translocation by NADH:ubiquinone oxidoreductase (complex I) from bovine heart mitochondria: does the enzyme operate by a Q-cycle mechanism? *Biochem. J.* 400, 541–550.
29. Clark, W. M. (1960) *Oxidation-reduction potentials of organic systems*, The Williams and Wilkins Company, Baltimore.
30. Horecker, B. L., and Kornberg, A. (1948) The extinction coefficients of the reduced band of pyridine nucleotides, *J. Biol. Chem.* 175, 385–390.
31. Woenckhaus, C., and Jeck, R. (1987) Preparation and properties of NAD and NADP analogues, in *Pyridine nucleotide coenzymes, chemical, biochemical and medical aspects* (Dolphin, D., Poulson, R., and Avramović, O., Eds.) pp 449–568, John Wiley & Sons, Toronto.
32. van Kuilenburg, A. B. P., Elzinga, L., van den Berg, A. A., Slingerland, R. J., and van Gennip, A. H. (1994) A fast and novel assay of CTP synthase: evidence for hysteretic properties of the mammalian enzyme, *Anticancer Res.* 14, 411–416.
33. Anderson, B. M., and Kaplan, N. O. (1958) Enzymatic studies with analogues of diphosphopyridine nucleotide, *J. Biol. Chem.* 234, 1226–1232.
34. Keister, D. L., and Hemmes, R. B. (1966) Pyridine nucleotide transhydrogenase from *Chromatium*, *J. Biol. Chem.* 241, 2820–2825.
35. Stocchi, V., Cucchiari, L., Canestrari, F., Piacentini, M. P., and Fornaini, G. (1987) A very fast ion-pair reversed-phase HPLC method for the separation of the most significant nucleotides and their degradation products in human red blood cells, *Anal. Biochem.* 167, 181–190.
36. Sazanov, L. A., and Hinchliffe, P. (2006) Structure of the hydrophilic domain of respiratory complex I from *Thermus thermophilus*, *Science* 311, 1430–1436.
37. Sled, V. D., Rudnitsky, N. I., Hatefi, Y., and Ohnishi, T. (1994) Thermodynamic analysis of flavin in mitochondrial NADH:ubiquinone oxidoreductase (complex I), *Biochemistry* 33, 10069–10075.
38. Briggs, G. E., and Haldane, J. B. S. (1925) A note on the kinetics of enzyme action, *Biochem. J.* 19, 338–339.
39. Chen, S., and Guillory, R. J. (1981) Studies on the interaction of arylazido- $\beta$ -alanyl NAD<sup>+</sup> with the mitochondrial NADH dehydrogenase, *J. Biol. Chem.* 256, 8318–8323.
40. Yamaguchi, M., Belogradov, G. I., and Hatefi, Y. (1998) Mitochondrial NADH-ubiquinone oxidoreductase (complex I) - effects of substrates on the fragmentation of subunits by trypsin, *J. Biol. Chem.* 273, 8094–8098.
41. Abdrakhmanova, A., Zwicker, K., Kerscher, S., Zickermann, V., and Brandt, U. (2006) Tight binding of NADPH to the 39 kDa subunit of complex I is not required for catalytic activity but stabilizes the multiprotein complex, *Biochim. Biophys. Acta* 1757, 1676–1682.
42. Hirst, J., Carroll, J., Fearnley, I. M., Shannon, R. J., and Walker, J. E. (2003) The nuclear encoded subunits of complex I from bovine heart mitochondria, *Biochim. Biophys. Acta* 1604, 135–150.
43. Zickermann, V., Zwicker, K., Tocilescu, M. A., Kerscher, S., and Brandt, U. (2007) Characterization of a subcomplex of mitochondrial NADH:ubiquinone oxidoreductase (complex I) lacking the flavoprotein part of the N-module, *Biochim. Biophys. Acta* 1767, 393–400.
44. Albracht, S. P. J., Mariette, A., and de Jong, P. (1997) Bovine heart NADH:ubiquinone oxidoreductase is a monomer with eight iron sulfur clusters and two FMN groups, *Biochim. Biophys. Acta* 1318, 92–106.
45. Hatefi, Y., and Bearden, A. J. (1976) Electron paramagnetic resonance studies on the reduction of the components of complex I and transhydrogenase-inhibited complex I by NADH and NADPH, *Biochem. Biophys. Res. Commun.* 69, 1032–1038.
46. Zharova, T. V., and Vinogradov, A. D. (1997) A competitive inhibition of the mitochondrial NADH-ubiquinone oxidoreductase (complex I) by ADP-ribose, *Biochim. Biophys. Acta* 1320, 256–264.
47. Vinogradov, A. D. (1993) Kinetics, control, and mechanism of ubiquinone reduction by the mammalian respiratory chain-linked NADH:ubiquinone reductase, *J. Bioenerg. Biomembr.* 25, 367–375.
48. Singh, A., Venning, J. D., Quirk, P. G., van Boxel, G. I., Rodrigues, D. J., White, S. A., and Jackson, J. B. (2003) Interactions between transhydrogenase and thio-nicotinamide analogues of NAD(H) and NADP(H) underline the importance of nucleotide conformational changes in coupling to proton translocation, *J. Biol. Chem.* 278, 33208–33216.
49. Fersht, A. R. (1998) *Structure and mechanism in protein science*, W. H. Freeman and Co., New York.
50. Avraam, R., and Kotlyar, A. B. (1991) Kinetics of NADH oxidation and NAD<sup>+</sup> reduction by mitochondrial complex I, *Biochemistry (Mosc.)* 56, 1181–1189.
51. Sled, V. D., and Vinogradov, A. D. (1993) Kinetics of the mitochondrial NADH-ubiquinone oxidoreductase interaction with hexaammineruthenium (III), *Biochim. Biophys. Acta* 1141, 262–268.
52. Vogel, R., Wiesinger, H., Hamprecht, B., and Dringen, R. (1999) The regeneration of reduced glutathione in rat forebrain mitochondria identifies metabolic pathways providing the NADPH required, *Neurosci. Lett.* 275, 97–100.
53. Rydström, J. (2006) Mitochondrial NADPH, transhydrogenase and disease, *Biochim. Biophys. Acta* 1757, 721–726.

BI7017915